

Stripeless incommensurate magnetism in a doped strongly correlated oxide

A. T. Savici,¹ I. A. Zaliznyak,¹ G. D. Gu,¹ and R. Erwin²

¹DCMPMS, Brookhaven National Laboratory, Upton, NY 11973

²NCNR, National Institute of Standards and Technology, Gaithersburg, MD 20899

(Dated: February 8, 2020)

We studied the nano-scale structure of the short-range incommensurate magnetic order in $\text{La}_{1.5}\text{Sr}_{0.5}\text{CoO}_4$ by elastic neutron scattering. Analysis of spatial anisotropy of diffuse scattering provides a clear test for popular stripe models where doped charges segregate forming lines along certain lattice direction(s). Imperfect stacking of these lines renders one-dimensional disorder and magnetic incommensurability to an otherwise robust antiferromagnetism of the un-doped material.

PACS numbers: 71.28.+d, 75.40.Cx, 75.40.Gb, 75.50.Ee

Ever since the advent of high-temperature superconductivity (HTSC) in cuprates, the physics of doped strongly correlated transition metal oxides remains at the forefront of condensed matter research [1, 2, 3]. In particular, there is a renewed interest in "colossal" magnetoresistance phenomena and in metal-insulator transitions associated with charge/orbital ordering in doped manganese and nickel oxides [3, 4, 5]. While macroscopic magnetic and transport properties of strongly correlated oxides respond to doping in many different and often fascinating ways, the appearance of structural and magnetic superlattice whose periods depend on the doping level is a common microscopic response shared by many oxides [6, 7, 8, 9, 10, 11, 12, 13, 14, 15].

Simultaneous incommensurate magnetic and charge ordering was probably first observed in a doped nickelate, $\text{La}_{2-x}\text{Sr}_x\text{NiO}_{4+y}$ [6]. It gained prominence when a similar phenomenon was discovered in a $x \approx 1/8$ doped cuprate with an anomalously suppressed superconductivity [7]. It was proposed that a simple model of real-space static ordering of holes and spins, where doped charges segregate into lines separating magnetically ordered stripe domains, can explain all features observed by elastic neutron scattering. In conjunction with earlier theoretical predictions of such superstructures in the 2D Hubbard model describing high- T_c cuprates [16, 17], striped phases gained broad popularity and became essentially a default model for describing incommensurate magnetic and charge superstructures in doped layered perovskite oxides $\text{La}_{2-x}\text{Sr}_x\text{MO}_4$ ($M = \text{Cu, Ni, Co, Mn}$).

There is a growing recognition, however, that physics of charge ordering in cuprates may differ significantly from that in well-insulating materials such as cobaltates and nickelates, where it can be viewed as ordering of polarons mainly driven by lattice elastic interactions [18, 19, 20]. In fact, it was argued theoretically that formation of superstructures whose period depends on the doping level, including stripes, is a natural response of a crystal lattice to the local strain associated with doped charges and can be already explained by considering the system's elastic energy [19]. Experiments indicate this type of superlattices in layered manganates and cobal-

tates [13, 14, 15].

In a superlattice associated with polaron ordering, atomic positions and/or alignment of magnetic moments do not vary in the direction perpendicular to propagation vector, presenting superlattice modulation as a periodic arrangement of lines of parallel spins and/or identical atomic displacements (Fig. 1). Hence, stripe superstructures resulting from one-dimensional electronic phase segregation and elastic/magnetic superlattices have similar appearance in real space. Accounting for domains, they also give rise to similarly positioned elastic peaks measured in scattering experiments. Is it possible to distinguish between the two cases? Here we show that for short-range superstructures this question can be answered by studying the nano-scale structure of disorder. By measuring pattern of elastic neutron scattering, we find that short-range incommensurate magnetism in half-doped cobaltite $\text{La}_{1.5}\text{Sr}_{0.5}\text{CoO}_4$ does not originate from an intrinsically one-dimensional stripe charge order.

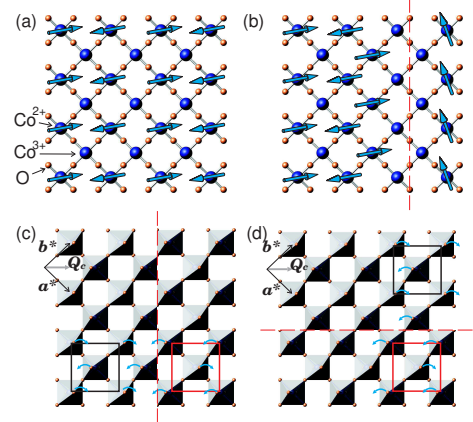


FIG. 1: (color) (a) Checkerboard charge and spin order at half-doping. (b) Stacking fault giving rise to short-range correlation and magnetic incommensurability in $\text{La}_{1.5}\text{Sr}_{0.5}\text{CoO}_4$ in stripe picture. (c), (d) LTO superlattice typical of weakly doped cuprates. \mathbf{a}^* , \mathbf{b}^* are reciprocal lattice vectors of the HTT phase, arrows show tilts of O octahedra. Stacking faults separating structural domains with opposite tilts (broken lines) running along "stripes" (perpendicular to Q_c), (c), and perpendicular to "stripes" (parallel to Q_c), (d), have the same energy, implying randomly shaped domains.

At half-doping, the system is naturally amenable to a checkerboard charge order (CO) where every other site in the $a-b$ plane of the high-temperature tetragonal (HTT) structure accommodates a hole, Fig. 1 (a). It is accompanied by a correlated harmonic modulation of atomic positions with propagation vector $Q_c = (1/2, 1/2)$ in the $a-b$ plane of the HTT reciprocal lattice. In stripe picture this type of CO is viewed as an alternate stacking of diagonal charge stripes. Structural disorder results from faults in stripe stacking, Fig. 1 (b), and is one-dimensional (1D) in nature. The ordering of small polarons driven by lattice strain, on the other hand, is in essence similar to the cooperative tilt pattern of oxygen octahedra in the low-temperature orthorhombic (LTO) lattice relieving chemical pressure in weakly doped cuprates, Fig. 1 (c,d). There, stacking faults have no intrinsic 1D rigidity and imply isotropic disorder.

We studied large single crystal of $\text{La}_{1.5}\text{Sr}_{0.5}\text{CoO}_4$ ($m \approx 11$ g) grown by floating zone method. It has a nearly HTT lattice with parameters $a = b \approx 3.83$ Å and $c \approx 12.5$ Å at $T = 10$ K [15]. Magnetic scattering reported here reveals a very slight LTO distortion such as shown in Fig. 1 (c,d), with $\Delta a_O/a_O \approx 0.6\%$. This is too small to be noticeable in structural Bragg scattering in our experiments, hence we retain the HTT notation. Measurements were done at NIST Center for Neutron Research, in $(h,k,0)$ and (h,h,l) zones, using cold (SPINS) and thermal (BT9) neutron triple axis spectrometers, respectively. Neutrons were monochromated by (002) reflection from vertically focussing pyrolytic graphite (PG) crystals and analyzed using flat PG(002) analyzers. Beryllium (SPINS) and PG (BT9) filters both before and after sample were used to remove contamination from higher order reflections in PG. On SPINS beam collimations were $\approx 37' - 80' - 80' - 240'$, from guide to detector, and neutron final energy was $E_f = 5$ meV. On BT9 we used $E_f = 14.7$ meV and collimations $\approx 40' - 40' - 40' - 100'$.

Color contour maps of the measured intensity are shown in Fig. 2 (a,b). In both $(h,k,0)$ (a) and (h,h,l) (b) zones peaks are much broader than full width at half maximum (FWHM) of the instrument resolution shown by ellipses. Peaks of magnetic origin are at $h,k \approx 0.25$ and 0.75 , while those due to atomic displacement accompanying charge ordering (CO) are at $h = k = 0.5$. Checkerboard CO in $\text{La}_{1.5}\text{Sr}_{0.5}\text{CoO}_4$ occurs at about 825 K, while magnetic ordering (MO) appears only around 30 K [15].

An appealing feature of stripe picture is that it can provide a simple real-space model explaining short-range incommensurate magnetism in nickelates, cuprates and cobaltites, and temperature-dependent CO incommensurability observed in nickelates [11]. In this picture they arise from discommensurations, or faults in the stacking pattern of 1D charge/spin stripes, favored by strong nearest-neighbor exchange coupling on the HTT square lattice, Fig. 1 (b). At half-doping such faults effectively reduce the average period of magnetic structure within

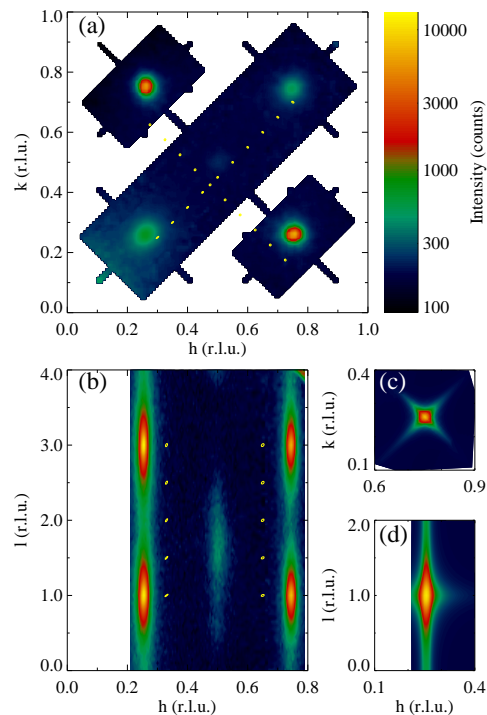


FIG. 2: (color) Contour map of neutron scattering intensity in $(h,k,0)$ (a) and (h,h,l) (b) zones at $T=3.5$ K and 10 K. Several resolution FWHM ellipses are shown. Magnetic peaks are at $h,k \approx 0.25, 0.75$ r.l.u. Charge order peak is seen at $h=k=0.5$ r.l.u. (c) and (d) Simulated intensity patterns for decoupled (stripe-like) correlations in $(h,k,0)$ and (h,h,l) zones.

the correlated domains in $a-b$ plane, consistent with slightly longer than $(1/4, 1/4)$ MO wave vector $Q_m \approx (0.256, 0.256)$ in $\text{La}_{1.5}\text{Sr}_{0.5}\text{CoO}_4$ [15]. It is also clear from the figure that discommensurations introduce linear disclinations parallel to stripes (coupling across two consecutive hole sites is weak and frustrated) and therefore truncate spin correlation range. Such disorder has a specific imprint in the structure of diffuse elastic peaks measured in scattering experiment [21, 22, 23, 24, 25].

Anisotropic short-range-ordered superlattices are well known in the physics of imperfect crystals and binary alloys such as Cu_3Au , [21, 22, 23, 24]. Phase mismatches at the boundaries of antiphase domains and/or stacking faults introduce one-dimensional disorder in the direction perpendicular to the defect planes. A combination of several systems of such phase slips allowed in the crystal structure leads to a peculiar X-ray scattering pattern, with tails along certain lattice directions [21, 23].

Similar considerations can be extended to scattering by short-range magnetic structures where disorder results from un-correlated stacking faults (disclinations) such as in Fig. 1 (b) [26]. The elastic magnetic neutron scattering cross section is given by

$$\frac{d\sigma(\mathbf{q})}{d\Omega} = N \left(\frac{r_m}{2\mu_B} \right)^2 \sum_j^N e^{-i\mathbf{q} \cdot \mathbf{R}_j} \langle \mathbf{M}_0^\perp(-\mathbf{q}) \mathbf{M}_j^\perp(\mathbf{q}) \rangle, \quad (1)$$

where $r_m \approx -5.39 \cdot 10^{-13} \text{cm}$, μ_B is the Bohr's magneton, $\mathbf{M}_j^\perp(\mathbf{q})$ is the Fourier-transform of the magnetization of atoms in the lattice unit cell at a position \mathbf{R}_j , projected perpendicular to wave vector \mathbf{q} and the sum extends over all N unit cells of the crystal. In the presence of long-range magnetic order with wave vector \mathbf{Q} ,

$$\langle \mathbf{M}_j(\mathbf{q}) \rangle = \mathbf{m}(\mathbf{q})e^{i\mathbf{Q} \cdot \mathbf{R}_j} + \mathbf{m}^*(\mathbf{q})e^{-i\mathbf{Q} \cdot \mathbf{R}_j}, \quad (2)$$

where order parameter $\mathbf{m}(\mathbf{q})$ incorporates Wannier function describing the unit cell magnetic form factor, and Eq. (1) gives a sum of delta-functions offset by \mathbf{Q} from reciprocal lattice points. Un-correlated magnetic disclinations in the crystal introduce additional random phase multipliers $e^{-i\phi_j}$ in the magnetization density (2). In view of its randomness, this phase factor can be decoupled in the correlation function in Eq. (1). Its statistical average is $\langle e^{-i\phi_j} \rangle = e^{-\langle \phi_j^2 \rangle / 2}$ (Bloch identity) and

$$\frac{d\sigma(\mathbf{q})}{d\Omega} = Nr_m^2 \left| \frac{\mathbf{m}^\perp(\mathbf{q})}{2\mu_B} \right|^2 \sum_j e^{-i\mathbf{q} \cdot \mathbf{R}_j - \frac{1}{2}\langle \phi_j^2 \rangle}. \quad (3)$$

In the case of planar (linear in 2D) disclinations perpendicular to principal lattice directions such as expected from stripes, the accumulated mean-square phase mismatch can be described by independent random walks along these directions. Then, $\langle \phi_j^2 \rangle / 2 = \sum_\alpha |n_{j,\alpha}| / \xi_\alpha$, where $n_{j,\alpha}$ label lattice sites, $\mathbf{R}_j = \sum_\alpha n_{j,\alpha} \mathbf{a}_\alpha$ and ξ_α are correlation lengths in appropriate units ($\alpha = x, y, z$). Substituting this into Eq. (1), one obtains cross-section in the form of a product of 1D lattice-Lorentzians,

$$\tilde{L}_{\xi_\alpha}(q_\alpha) \equiv \frac{\sinh \xi_\alpha^{-1}}{\cosh \xi_\alpha^{-1} - \cos(q_\alpha \pm Q_\alpha)}, \quad (4)$$

along principal crystallographic directions. Eq. (4) is just a sum of Lorentzians placed periodically in reciprocal lattice. Factorized cross-section is a consequence of the 1D nature of disorder generated by system of linear/planar phase slips. It retains the orientational symmetry of these defects in the crystal lattice, Fig. 2 (c,d).

If, perhaps upon appropriate re-scaling of co-ordinates, the disorder is isotropic, such as introduced for example by the domain structure in the (anisotropic) random field Ising model (RFIM) [27], phase slips depend only on $|\mathbf{R}_j|$ and $\langle \phi_j^2 \rangle / 2 = \frac{|\mathbf{n}_j|}{\xi}$. While the lattice sum can not be easily evaluated in this case, it can be rewritten as a sum of integrals repeated periodically in reciprocal lattice, so as to restore the lattice translational symmetry. For a D -dimensional lattice ($D = 1, 2, 3$) this gives a generalized-lattice-Lorentzian function

$$\sum_{\boldsymbol{\tau}} \left(1 + \sum_{\alpha=1}^D (q_\alpha \pm Q_\alpha + \tau_\alpha)^2 \xi_\alpha^2 \right)^{-\frac{D+1}{2}}, \quad (5)$$

where ξ_α are the original un-rescaled correlation lengths, and $\boldsymbol{\tau}$ are reciprocal lattice vectors.

TABLE I: Scattering functions for different structure of the nano-scale disorder on a 3D lattice (assuming large ξ_α) and the corresponding χ^2 obtained from fitting our data (see text).

type of disorder	scattering cross section	χ^2
1D×1D×1D	$(1 + q_1^2 \xi_1^2)^{-1} (1 + q_2^2 \xi_2^2)^{-1} (1 + q_3^2 \xi_3^2)^{-1}$	13.6
2D×1D	$(1 + q_1^2 \xi_1^2 + q_2^2 \xi_2^2)^{-1.5} (1 + q_3^2 \xi_3^2)^{-1}$	10.2
3D	$(1 + q_1^2 \xi_1^2 + q_2^2 \xi_2^2 + q_3^2 \xi_3^2)^{-2}$	6.4

Scattering functions for different combinations of disorder described by Eqs. (4) and (5) on a 3D lattice are summarized in Table I (for large ξ_α only one term in the lattice sum is important). A fully factorized 1D×1D×1D cross-section (product of 1D Lorentzians in all 3 directions) can be expected in the stripe picture for $\text{La}_{1.5}\text{Sr}_{0.5}\text{CoO}_4$. Resulting diffuse scattering has a diamond-like shape, reminiscent of a superposition of quasi-1D "rods" of scattering extended perpendicular to stripes and/or planes, Fig. 2 (c,d).

From comparing Fig. 2 (a,b) and (c,d) it is already clear that short-range magnetic order in $\text{La}_{1.5}\text{Sr}_{0.5}\text{CoO}_4$ is not caused by random one-dimensional magnetic disclinations associated with stripes running along diagonal of the HTT unit cell as in Fig. 1 (b). This can be further quantified by fitting the 1D scans perpendicular to this direction made at different off-sets δq from magnetic peak in the orthogonal direction to cross-sections shown in Table 1, Fig. 3 (a). "Correlation lengths" obtained from such fits of scans along (h,h,0) and (0,0,l) are shown in Fig. 3 (b,c). For a factorized scattering cross-section they should be ξ_α , independent of δq , while for the cross-section of Eq. (5) with $D > 1$,

$$\xi_\alpha^{fit} = \frac{\xi_\alpha}{\sqrt{1 + (\tilde{\xi} \delta q)^2}}. \quad (6)$$

Variation of the fitted correlation length ξ_{ab}^{fit} in Fig. 3 (b) is clearly inconsistent with the factorized scattering cross-section expected for disclinations associated

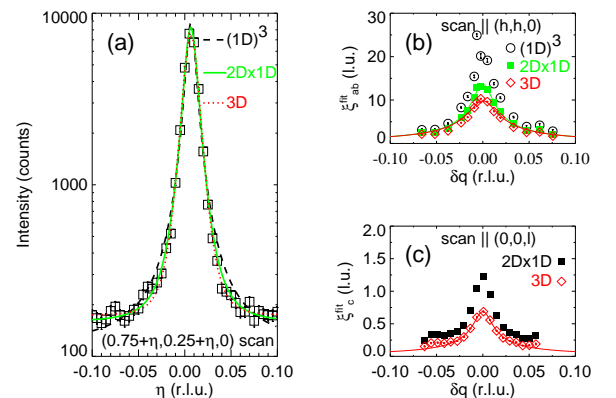


FIG. 3: (color) (a) Typical scan through magnetic peak with fits to all 3 cross-sections of Table 1. For a single scan the lineshapes are barely distinguishable. (b) and (c) "correlation length" for each scan as a function of its distance δq from magnetic peak position, $\mathbf{Q}_m = (0.255, 0.255, 1) + \boldsymbol{\tau}$. The solid/dashed lines are fits to Eq. 6, varying ξ_α and $\tilde{\xi}$.

with stripes in the $a-b$ plane. Moreover, ξ_c^{fit} obtained from measurements around $(1/4, 1/4, 1)$ in the (h, k, l) zone shown in Fig. 3 (c) indicates that factorization into a 2D dependence in $a-b$ plane and a 1D dependence along c -axis arising from independent faults in plane stacking is also improbable. Therefore, our results must be best described by Eq. (5) with $D=3$ and anisotropic correlation lengths, indicating disorder typical of an anisotropic 3D random field Ising model [27]. This is confirmed by fitting the entire data set to resolution corrected cross sections. The obtained χ^2 are shown in Table I. With only one flat background and one intensity prefactor per experiment, magnetic peak position \mathbf{Q}_m and correlation lengths varied in magnetic cross-section, the best global fit ($\chi^2 = 6.4$) is achieved for a cross-section with 3D disorder, with $\xi_{ab} = 13.3$ and $\xi_c = 0.58$ (r.l.u.), Fig. 4.

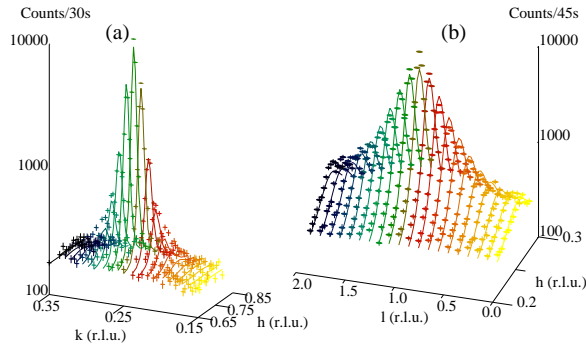


FIG. 4: (color) Elastic neutron scattering from $\text{La}_{1.5}\text{Sr}_{0.5}\text{CoO}_4$. (a) $(h, k, 0)$ orientation, (b) (h, h, l) orientation. The lines show fit to Eq. (5) describing coupled anisotropic 3D correlations.

In summary, incommensurate magnetic and charge superstructures observed in hole-doped cuprates, nickelates and cobaltates $\text{La}_{2-x}\text{Sr}_x\text{MO}_4$ ($M = \text{Cu}, \text{Ni}, \text{Co}, \text{Mn}$) are often described in terms of discommensurations in the quasi-regular stacking of charge lines separating antiferromagnetically ordered stripe domains. Existence of such faults in stripe stacking has two essential consequences. First, it renders the super-lattice incommensurability, which can explain the temperature-dependent incommensurate magnetism observed in hole-doped nickelates with $0.25 \lesssim x \lesssim 0.5$ [11, 12]. Secondly, stacking faults truncate the super-lattice coherence, resulting in a short-range glassy superstructure which manifests itself in experiment by finite-width, diffuse peaks of elastic scattering in place of Bragg reflections.

Experimental study of short-range magnetic and/or charge scattering such as presented in this letter provides a clear test for stripe picture. Our results show conclusively that stripe-type superstructure is not at the origin of magnetic incommensurability in the half-doped cobaltate $\text{La}_{1.5}\text{Sr}_{0.5}\text{CoO}_4$. This is not completely unexpected, as charge order in this material occurs independently of

spin order, in a well-insulating state and at much higher temperature [15]. It is mainly driven by lattice electrostatics and local spin entropy coupled to the crystal field level splitting of Co ions. The rigidity of quasi-1D charge-stripe segregation, on the other hand, is rendered by the gain in kinetic energy of charge hopping [7, 16, 17], which seems insignificant in $\text{La}_{1.5}\text{Sr}_{0.5}\text{CoO}_4$. Our analysis can be applied for probing the relevance of kinetic energy driven "parallel" and "diagonal" stripe phases for CO in cuprates and related insulating $\text{La}_{2-x}\text{Sr}_x\text{MO}_4$ oxides.

We thank NIST Center for neutron Research for hospitality and J. Tranquada and M. Hucker for discussions. This work was performed under Contract DE-AC02-98CH10886, US Department of Energy, and utilized facilities supported in part by the National Science Foundation under Agreement DMR-0454672.

- [1] P. A. Lee, *et al.*, Rev. Mod. Phys. **78**, 17 (2006).
- [2] J. Orenstein and A. J. Millis, Science **288**, 468 (2000).
- [3] Y. Tokura, Physics Today **7**, 50 (2003).
- [4] Y. Tokura and N. Nagaosa, Science **288**, 462 (2000).
- [5] M. Imada, *et al.*, Rev. Mod. Phys. **70**, 1039 (1998).
- [6] J. M. Tranquada, *et al.*, Phys. Rev. Lett. **73**, 1003 (1994).
- [7] J. M. Tranquada, *et al.*, Nature **375**, 561 (1995); Phys. Rev. B **54**, 7489 (1996).
- [8] B. O. Wells, *et al.*, Science **277**, 1067 (1997).
- [9] C. H. Chen, *et al.*, Phys. Rev. Lett. **71**, 2461 (1993).
- [10] H. Yoshizawa, *et al.*, Phys. Rev. B **61**, R854 (2000).
- [11] R. Kajimoto, *et al.*, Phys. Rev. B **64**, 144432 (2001); Phys. Rev. B **67**, 014511 (2003).
- [12] K. Ishizaka, *et al.*, Phys. Rev. B **67**, 184418 (2003); Phys. Rev. Lett. **92**, 196404 (2004).
- [13] S. Larochelle, *et al.*, Phys. Rev. Lett. **87**, 095502 (2001); Phys. Rev. B **71**, 024435 (2005).
- [14] N. Sakiyama, *et al.*, unpublished.
- [15] I. A. Zaliznyak, *et al.*, J. Appl. Phys. **95**, 7369 (2004).
- [16] J. Zaanen, O. Gunnarsson, Phys. Rev. B **40**, 7391 (1989).
- [17] V. J. Emery, S. A. Kivelson, Physica C **209**, 597 (1993).
- [18] J. Zaanen, P. B. Littlewood, Phys. Rev. B **50**, 7222 (1994).
- [19] Europhys. Lett., **55**, 208 (2001).
- [20] E. Collart, *et al.*, Phys. Rev. Lett. **96**, 157004 (2006).
- [21] J. M. Cowley, J. Appl. Phys. **21**, 24 (1950).
- [22] A. J. C. Wilson, Proc. Roy. Soc. **A180**, 277 (1942); *ibid.* **A181**, 360 (1943).
- [23] B. E. Warren, *X-ray Diffraction* (Dover Publications, Inc., New York, 1990).
- [24] M. A. Krivoglaz, *X-ray and Neutron Diffraction in Non-ideal Crystals* (Springer, New York, 1996).
- [25] Y. Chen, *et al.*, Phys. Rev. B **72**, 184401 (2005).
- [26] I. A. Zaliznyak and S.-H. Lee, in *Modern Techniques for Characterizing Magnetic Materials*, Ed. Y. Zhu (Springer, New York, 2005).
- [27] O. Zachar, I. Zaliznyak, Phys. Rev. Lett. **91**, 036401 (2003).